



Publication Year	2016
Acceptance in OA	2020-05-29T07:15:37Z
Title	Kinematics and Magnetic Properties of a Light Bridge in a Decaying Sunspot
Authors	FALCO, MARIACHIARA, Borrero, J. M., Guglielmino, S. L., ROMANO, Paolo, Zuccarello, Francesca, Criscuoli, S., Cristaldi, A., ERMOLLI, Ilaria, Jafarzadeh, S., Rouppe van der Voort, L.
Publisher's version (DOI)	10.1007/s11207-016-0944-8
Handle	http://hdl.handle.net/20.500.12386/25283
Journal	SOLAR PHYSICS
Volume	291

Kinematics and Magnetic Properties of a Light Bridge in a Decaying Sunspot

M. Falco^{1,2} · J.M. Borrero³ · S.L. Guglielmino¹ ·
P. Romano⁴ · F. Zuccarello¹ · S. Criscuoli⁵ ·
A. Cristaldi² · I. Ermolli² · S. Jafarzadeh⁶ ·
L. Rouppe van der Voort⁶

Received: 29 October 2015 / Accepted: 16 June 2016 / Published online: 8 July 2016
© Springer Science+Business Media Dordrecht 2016

Abstract We present the results obtained by analysing high spatial and spectral resolution data of the solar photosphere acquired by the *CRisp Imaging SpectroPolarimeter* at the *Swedish Solar Telescope* on 6 August 2011 of a large sunspot with a light bridge (LB) observed in NOAA AR 11263. These data are complemented by simultaneous *Hinode Spectropolarimeter* (SP) observation in the Fe I 630.15 nm and 630.25 nm lines. The continuum intensity map shows a discontinuity in the radial distribution of the penumbral filaments in correspondence with the LB, which shows a dark lane ($\approx 0.3''$ wide and $\approx 8.0''$ long) along its main axis. The available data were inverted with the Stokes Inversion based on Response functions (SIR) code and physical parameters maps were obtained. The line-of-sight (LOS) velocity of the plasma along the LB derived from the Doppler effect shows motions towards and away from the observer up to 0.6 km s^{-1} that are lower in value than the LOS velocities observed in the neighbouring penumbral filaments. The noteworthy result is that we find motions towards the observer of up to 0.6 km s^{-1} in the dark lane where the LB is located between two umbral cores, while the LOS velocity motion towards the observer is strongly reduced where the LB is located between an umbral core at one side and penumbral filaments on the other side. Statistically, the LOS velocities correspond to upflows or downflows, and comparing these results with *Hinode*/SP data, we conclude that the surrounding magnetic field configuration (whether more or less inclined) could have a role in maintain-

✉ M. Falco
mfalco@oact.inaf.it

¹ Dipartimento di Fisica e Astronomia – Sezione Astrofisica, Università di Catania, via S. Sofia 78, 95123 Catania, Italy

² Osservatorio Astronomico di Roma, Istituto Nazionale di Astrofisica (INAF), Via Frascati 33, 00078 Monte Porzio Catone, Italy

³ Kiepenheuer-Institut für Sonnenphysik, Schöneckstr (KIS), 6, 79110 Freiburg, Germany

⁴ Osservatorio Astrofisico di Catania, Istituto Nazionale di Astrofisica (INAF), via S. Sofia 78, 95123 Catania, Italy

⁵ National Solar Observatory (NSO), Sacramento Peak Box 62, Sunspot, NM 88349, USA

⁶ Institute of Theoretical Astrophysics, University of Oslo, P.O. Box 1029, Blindern, 0315 Oslo, Norway

ing the conditions for the process of plasma pile-up along the dark lane. The results obtained from our study support and confirm outcomes of recent magneto-hydrodynamic simulations showing upflows along the main axis of an LB.

Keywords Sun: photosphere · Sun: magnetic fields · Sun: sunspots · Sun: high resolution observations

1. Introduction

In recent years, our understanding of the physical mechanisms responsible for the formation and evolution of sunspots has been greatly improved thanks to polarimetric data with high temporal, spatial, and spectral resolution. These observations have unveiled some physical properties of several fine structures of sunspots (Thomas and Weiss, 2004; Borrero and Ichimoto, 2011; Rempel and Schlichenmaier, 2011), such as umbral dots (inside the umbra), dark-core filaments (in the penumbra), and light bridges (LBs, separating some umbral portions).

The study of the LBs plays an important role for understanding the growing and decay phases of sunspots. LBs are bright and elongated structures delineating the border between dark umbral cores. In some cases they form during the coalescence of sunspots, while in other cases they are evidence of re-established granular motions within the spot, and often indicate the beginning of spot fragmentation (Vazquez, 1973). Moreover, before the formation of an LB, several umbral dots emerge in the location where an LB will be formed, and the LB structure rapidly intrudes from the leading edge of penumbral filaments into the umbra (Katsukawa *et al.*, 2007).

According to Thomas and Weiss (2004), there are two types of LBs: those that are segmented along their length, with bright segments resembling tiny granules separated by narrow dark lanes oriented perpendicular to the axis of the LB (Berger and Berdyugina, 2003); and those that are unsegmented, and, according to Lites *et al.* (2004), resemble the elongated features seen in the penumbra. Moreover, LBs are classified into faint light bridges (FLBs), which are narrow bright features inside the umbra, and strong light bridges (SLBs), separating different umbral fragments (Sobotka, Bonet, and Vazquez, 1994). LBs often exhibit a granular morphology, even if the size, lifetime, and brightness of these granules are different from those found in the granulation of the quiet photosphere. In particular, the granular structures forming SLBs are generally smaller than those in the quiet photosphere: the typical sizes are 1.2'' (Sobotka, Bonet, and Vazquez, 1994), instead of 1.5''. The intensity of the LB granules is about 85% of the mean photospheric intensity. By following the temporal evolution of these sub-structures during their irregular motions inside the LB, proper motions with velocities up to 1.5 km s⁻¹ have been detected (Hirzberger *et al.*, 2002). The lifetime distribution of these granular features shows a maximum at 5 min and a second peak at approximately 20 min (Hirzberger *et al.*, 2002).

The magnetic fields in LBs are weaker, sparser, and more horizontal than in the neighbouring umbrae. LBs with their weak and inclined fields therefore represent a discontinuity in the regular umbral field (Lites *et al.*, 1991; Leka, 1997). Recent observations by Jurčák, Sobotka, and Martínez Pillet (2005) and Jurčák, Martínez Pillet, and Sobotka (2006) pointed out an essentially field-free region at the deepest visible level of two LBs, but with magnetic canopies spreading from either sides of the LBs and merging above them.

Many segmented LBs also show a narrow dark lane along their main axis (Rimmele, 2008). Berger and Berdyugina (2003) showed that this lane has a typical width that varies

from $0.2''$ to $0.5''$: in the larger section the features (the granules along the sides of the lane) resemble large-scale modified convection, while in the smaller sections of the LB, the granules appear increasingly smaller, until only a central dark lane is observed, probably due to the alignment of convection cells caused by the magnetic field. During its lifetime, portions of the dark lane often dissolve and then reform again (Rimmele, 2008).

An analysis of an LB velocity field carried out by Rimmele (1997) provided evidence of sinking plasma in the axial channel. From the correlation between vertical velocity and continuum intensity in the granules belonging to an LB, Rimmele (1997) could confirm their convective origin. In this regard, it is important to find out whether the motions observed in LBs have a magneto-convective origin or are due to convection penetrating from the sub-photospheric layers into a field-free gap (Thomas and Weiss, 2004). Furthermore, this study is also important to understand the physical processes at the basis of the sunspot formation. There are two theoretical models that attempt to describe the sunspot formation process: the monolithic model (Cowling, 1957) and the spaghetti-like model (Parker, 1979a,b,c), but according to Rempel and Schlichenmaier (2011), it seems that the monolithic model is favoured.

More recent observations show that in segmented LBs the dark lane is characterised by upflows, while in the intergranular lanes of normal granulation we can see downflows (Roupe van der Voort, Bellot Rubio, and Ortiz, 2010). Therefore, the process that generates the dark lane seems to be plasma pile-up caused by the strong decrease of the vertical upflow near the surface. The plasma is forced by the cusp-like surrounding magnetic field into a region with enhanced density and therefore higher opacity (Giordano *et al.*, 2008). This pushes the elevation of the $\tau = 1$ (where τ denotes the optical depth) surface into a cooler, higher part of the atmosphere, resulting in a dark lane in intensity images (Schüssler and Vögler, 2006). Moreover, recent observations have also revealed that some types of LBs are accompanied by remarkable long-lasting plasma ejections or surge activities in the chromosphere (Asai, Ishii, and Kurokawa, 2001; Shimizu *et al.*, 2009; Shimizu, 2011; Louis, Beck, and Ichimoto, 2014; Toriumi, Katsukawa, and Cheung, 2015).

In this article we provide a further observational contribution to the understanding of plasma motions and magnetic fields in an LB by using a very high-quality dataset acquired with the *CRisp Imaging SpectroPolarimeter* on the 1-m *Swedish Solar Telescope* on 6 August 2011, imaging NOAA AR 11263. In the next section we describe the dataset and the methods. In Section 3 we report our results, in Section 4 we interpret them, and in Section 5 we draw our conclusions.

2. Observations and Data Analysis

Active Region NOAA AR 11263 was observed on 6 August 2011 at N16W43 ($\mu = 0.76$, which is the value of the cosine of the heliocentric angle θ of the observations) using the *CRisp Imaging SpectroPolarimeter* (CRISP; Scharmer *et al.*, 2008) mounted at the 1-m *Swedish Solar Telescope* (SST; Scharmer *et al.*, 2003), during a joint observing campaign (HOP 0195) with the *Hinode* satellite (Kosugi *et al.*, 2007). The CRISP spectropolarimetric measurements were taken from 09:53:32 UT to 10:48:43 UT along the Fe I line pair at 630.15 nm and 630.25 nm with 15 spectral points for each line, in steps of 4.4 pm from -26.8 pm to 34.8 pm for 630.15 nm and steps of 4.4 pm from -30.8 pm to 30.8 pm for 630.25 nm with respect to the line centre of each line. Cristaldi *et al.* (2014) used the same type of dataset for a different target observed during this observing campaign. The average cadence of each scan was 28 seconds. Liquid crystals modulated the light cycling

through four polarisation states (I , Q , U , and V) (Schnerr, de La Cruz Rodríguez, and van Noort, 2011), and five exposures per polarisation state were acquired, resulting in a total of 20 exposures per line position. The pixel size of the CRISP cameras was $0.06'' \text{ pixel}^{-1}$ at 630.15 nm and 630.25 nm. The noise level is different for each Stokes parameter: $4 \times 10^{-3} I/I_c$ (where I_c is the mean quiet-Sun continuum intensity value) for Stokes Q , $3 \times 10^{-3} I/I_c$ for Stokes U , and $8 \times 10^{-3} I/I_c$ for Stokes V . The field of view (FOV) of these SST measurements was $57.5'' \times 57.3''$.

Moreover, the dataset acquired by the *Hinode* satellite during the joint observing campaign was used to obtain information on the magnetic field topology of the AR. The *Hinode*/SP (Tsuneta *et al.*, 2008; Lites *et al.*, 2013) recorded the Stokes profiles along the Fe I line pair at 630.15 nm and 630.25 nm with a pixel sampling of $0.317''$ and a noise level of about $10^{-3} I/I_c$ (fast mode). Level 2 data obtained from the Milne–Eddington gRid Linear Inversion Network (MERLIN) code (Lites *et al.*, 2007) were used in our analysis. We applied the Non-Potential magnetic Field Calculation technique (NPFC; Georgoulis, 2005) on the inverted dataset to perform azimuth disambiguation in solar vector magnetograms, obtaining inclination and azimuthal angle maps in the local solar frame.

To follow the global evolution of the AR and the formation of the LB, we also analysed continuum images and line-of-sight (LOS) magnetograms in the Fe I line at 617.3 nm from 2 to 7 August 2011 taken by the *Helioseismic and Magnetic Imager* (HMI; Scherrer *et al.*, 2012) onboard the *Solar Dynamics Observatory* (SDO; Pesnell, Thompson, and Chamberlin, 2012). Both datasets were characterised by a pixel size of $0.5''$ and a time cadence of 2 hours.

The SST data were processed using the Multi-Object Multi-Frame Blind Deconvolution (MOMFBD; van Noort, Rouppe van der Voort, and Löfdahl, 2005) technique to achieve the highest spatial resolution in combination with the adaptive optics. For the data processing we followed the different steps in the CRISPRED reduction pipeline for CRISP data (de la Cruz Rodríguez *et al.*, 2015). Wideband images, acquired simultaneously with the spectro-polarimetric scans, were used as a so-called anchor channel in the reduction procedure to ensure precise alignment between the sequentially recorded CRISP narrowband images. Following the data calibration, we obtained two three-dimensional datacubes containing restored, aligned data with a high angular resolution of $0.16''$. The blueshift variation from the centre of the FOV towards the edge, which is due to the Fabry–Pérot system, was corrected during the reduction procedure.

We applied the Stokes Inversion based on Response functions (SIR; Ruiz Cobo and del Toro Iniesta, 1992) code to the SST sequence acquired at 10:17 UT, obtained during the best seeing condition, to create maps of the magnetic field strength and temperature in a sub-array FOV centred on the LB region. Using the SIR code, we simultaneously inverted the spectra acquired in the two lines of the Fe I line pair at 630.1/630.2 nm. Stokes I values in the red wing of the Fe I 630.25 nm line were not included in the profile of the inverted pixels because the signal is altered by telluric lines and, for low temperatures, by molecular blends. We used two different models as initialisation of the inversion, depending on the region, identified by a threshold in the continuum intensity, forming the FOV: a penumbral model ($0.4 < I/I_c < 0.8$) and an umbral model ($I/I_c < 0.4$). In the penumbral model, we changed the temperature (T) and the electron pressure (p_{e-}) using the values described by del Toro Iniesta, Tarbell, and Ruiz Cobo (1994), and we used a value of 1000 G for the magnetic field strength and 1.0 km s^{-1} for the LOS velocity. For the umbral model we used the T and p_{e-} values provided by Collados *et al.* (1994) (corresponding to an umbral model for a small spot), and we used a constant value of 2000 G for the magnetic field strength as an initial guess. The temperature stratification of each component was modified with two nodes.

The other physical parameters (magnetic field, LOS velocity, inclination, and azimuth angles) were assumed to be constant with height (number of nodes equal to one). We used the Milne–Eddington-like approximation to estimate the average physical parameters over the range of line formation heights. A fixed macroturbulence velocity of 2.95 km s^{-1} was used to mimic the effects of the spectral point spread function (PSF) of the instrument. A fixed filling factor of one was used for the inversion. The straylight contamination was not considered during the inversion because the Stokes I profile in the Fe I line at 630.2 nm is heavily affected by blends, thereby severely affecting our ability to determine its contribution. We decided to apply more weight to Q , U , and V Stokes parameters, by a factor of four with respect to Stokes I owing to the larger noise in the intensity than in the polarisation profiles. Therefore, due to the uncertainties that could affect the velocity values derived from the SIR inversion, we decided to derive the Doppler velocity by applying a Gaussian fit to the Fe I line profile at 630.15 nm. Moreover, the CRISP dataset was not used to study the inclination angle because the LB FOV was not sufficient to apply the NonPotential magnetic Field Calculation (NPFC) code.

To study the kinematics in the LB region, we obtained the Doppler velocity of plasma motions by applying a Gaussian fit to the Fe I line profile at 630.15 nm with the MPFIT routine to five sequences of the SST dataset (Markwardt, 2009) in the Interactive Data Language (IDL). The values of LOS velocity were deduced from the Doppler shift of the centroid of the fitted line profiles in each spatial point. The LOS velocity map was calibrated by subtracting the mean velocity of the pixels of the umbra in the FOV (pixels whose threshold of the continuum intensity is lower than $0.4 I/I_c$), assuming that the umbra of the sunspot was at rest, according to Balthasar and Schmidt (1993). We estimated the uncertainty affecting the velocity measurements considering the standard deviation of the centroids of the line profiles estimated in all points of the FOV. Thus, the estimated relative error in the velocity is $\pm 0.2 \text{ km s}^{-1}$. Moreover, we recall that given the position of AR 11263 at N16W43, the measured LOS velocities do not correspond to velocities perpendicular to the solar surface.

3. Results

Figure 1 shows the HMI/SDO continuum image and the corresponding magnetogram taken on 6 August 2011 for NOAA AR 11263. On this day, the AR was characterised by a preceding main negative polarity sunspot showing a light bridge and by several smaller positive polarity ones (see left and right panels of Figure 1).

Figure 2 shows the evolution of the preceding spot from 3 to 6 August 2011. The well-defined umbra and penumbra (Figure 2, top left panel) start to fragment on 4 August, when the penumbral filaments in the north-western part of the spot seem to penetrate the umbral region (see the red contour in Figure 2, top right panel). On 5 August (Figure 2, bottom left panel), the preceding sunspot exhibits two umbrae with different shapes, one more elongated and the other with a more circular shape, inside the same penumbra. The LB appears and completes its formation on 6 August, before the start of the CRISP observations analysed in the following (the CRISP FOV is indicated by the box in Figure 2, right bottom panel).

Figure 3 shows the continuum intensity map observed by CRISP on 6 August at 10:17 UT, with the LB oriented approximately along the north-south direction. It is worth noting that the radial distribution of the penumbral filaments is modified in the regions near the LB. Penumbral filaments south of the LB are smaller than the others around the sunspot. Moreover, in this area the photospheric granulation seems to prevail over the penumbra.

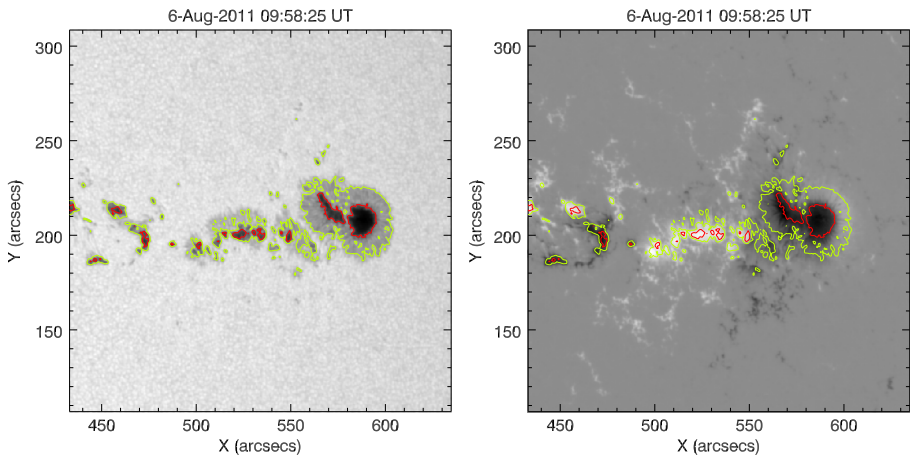


Figure 1 Continuum intensity map (left panel) and LOS magnetogram (right panel) of NOAA AR 11263 obtained by the HMI/SDO in the Fe I 617.3 nm line on 6 August 2011. The red and green contours indicate the umbral and penumbral borders, as derived by applying an intensity threshold set to $I/I_c = 0.5$ and $I/I_c = 0.9$, respectively, and where I_c is the mean quiet-Sun continuum intensity value. North is at the top, west is at the right.

Furthermore, to the north-east of the LB we note some small dark regions characterised by a local higher value of the magnetic field strength (compare with Figure 4, top panel).

In Figure 4 we show the magnetic field strength and inclination angle maps in the local solar frame obtained by the MERLIN inversion on *Hinode*/SP data. In the bottom panel 0° and 180° correspond to a radially outward and inward magnetic field, respectively. The magnetic field strength map indicates that in the LB region the magnetic field strength is lower than in the surroundings. The inclination map shows an inclination angle lower than the magnetic field inclination of the two umbral zones in the region of the LB, where it is $\approx 180^\circ$. These lower inclination angles are more evident between $210''$ and $220''$ in the y direction, corresponding to the northern part of the LB.

We restricted our analysis of the LB properties to the data acquired by CRISP/SST at 10:17 UT in the FOV indicated by the box reported in Figures 3 and 4. We divided the LB into two parts, characterised by a different configuration of the magnetic field at its sides: the northern part (corresponding to the upper part of the LB and indicated by LB_n in Figures 5 and 6) with the larger umbral core of the spot at the eastern side and the penumbral filaments at the opposite side (compare with Figure 3), and the southern part (corresponding to the bottom part of the LB and indicated by LB_s in Figures 5 and 6) with the two umbral cores at both sides.

In Figure 5 (top panel) we show a $\approx 90^\circ$ rotated zoomed image of the LB region displayed in Figure 3 (white box), where the black line indicates the dark lane of the LB. The narrow dark lane along the main axis of the LB has an average width of $0.3''$ and a length of about $8.0''$. It seems to connect two dark penumbral filaments located on both sides of the LB. Moreover, the LB appears to be segmented along its length by tiny granules (sizes from $0.2''$ to $0.8''$) separated by narrow dark lanes oriented perpendicularly to the LB axis. In the other panels of Figure 5 we plot the LOS velocity along the dark lane measured around the time of the best seeing sequence (10:17:05 UT). These plots show that in the LB_n region, the LOS velocity values are between 0 and -0.2 km s^{-1} (negative velocity values indicate motions

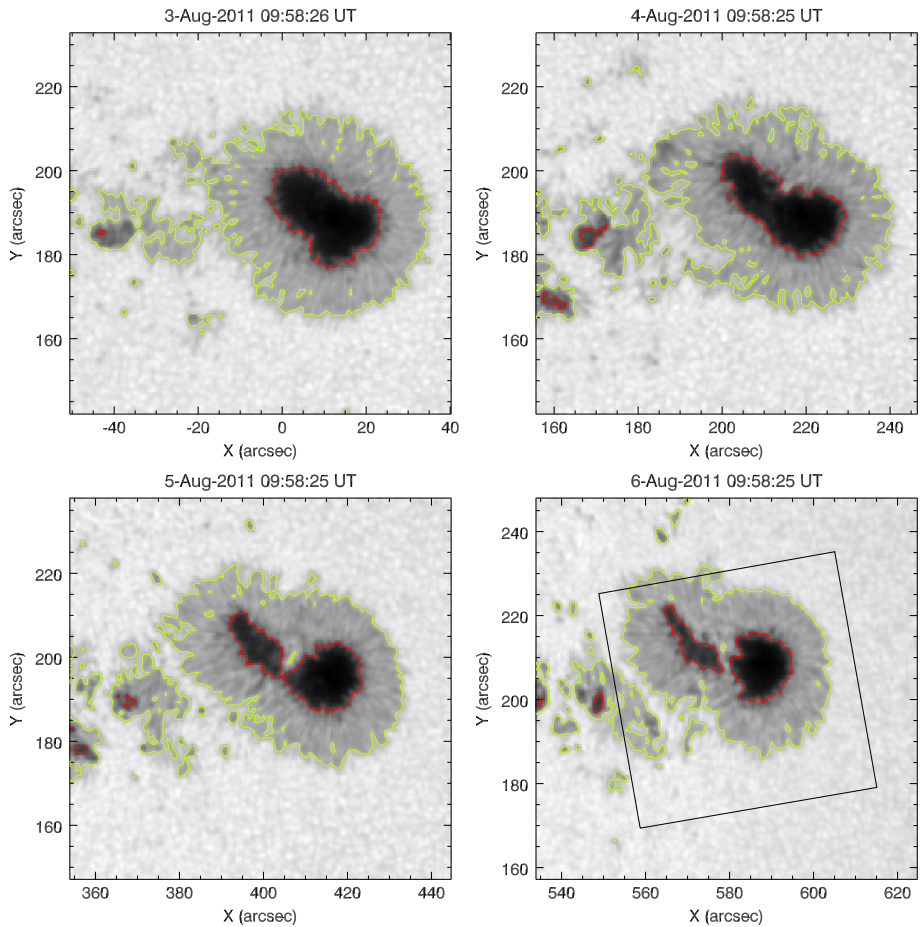


Figure 2 HMI/SDO images in the continuum of the Fe I line at 617.3 nm of the preceding sunspot of NOAA AR 11263 taken on consecutive days, from 3 to 6 August 2011. The FOV is $\approx 90 \times 90$ arcsec. The colour contours have the same meaning as in Figure 1. The sequence shows the evolution of the sunspot umbra and the formation of the LB. The box in the bottom right panel indicates the FOV of the CRISP observations analysed in our study and shown in Figure 3.

toward the observer), while in the LB_s region, the LOS velocity is higher, up to -0.8 km s^{-1} . Therefore, we note that the dark lane shows mostly motions toward the observer, which appear to be higher in LB_s where the LB is located between two umbral regions. We can see that this trend of the LOS velocity along different portions of the LB persists at least for 4–5 minutes, i.e., for a lifetime comparable with the lifetime of the LB granules.

To investigate how the configuration of the magnetic field at the LB sides can influence the dark lane properties, we therefore studied the intensity, the magnetic field strength, the temperature, and the LOS velocity inside and around the LB at 10:17:05 UT (see Figure 6) with particular attention to the vertical segments reported in Figure 5 (bottom panel), where the LOS velocities of the dark lane are completely different.

The granules at the western side of the LB_n (see the white arrow in the LB_n portion in Figure 6, top left panel) are larger than those at the eastern side (conversely in the southern

Figure 3 Continuum intensity map of the preceding sunspot of NOAA AR 11263 obtained by CRISP at the Fe I 630.15 nm line on 6 August 2011 at 10:17 UT. The solid box indicates the LB FOV analysed in the text. The arrow points in the direction of the disk centre.

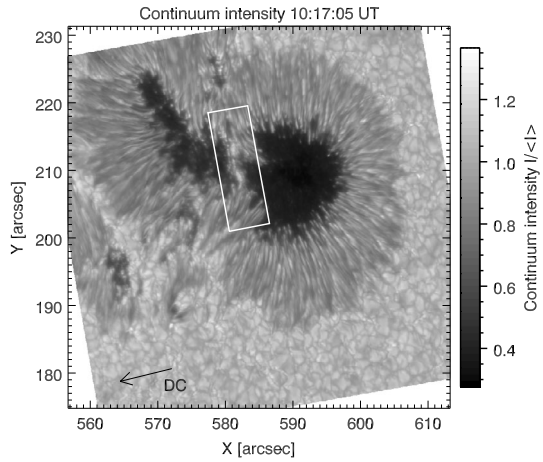


Figure 4 Maps of the magnetic field strength and inclination angle in the local solar frame coordinate obtained from inverting both the Fe I 630.15 nm and 630.25 nm line datasets taken by *Hinode* on 6 August 2011 at 10:05:06 UT. The region with $X > 606''$ is not covered by *Hinode* observations. In the bottom panel 0° and 180° correspond to the directions of radially outward and inward magnetic field, respectively. In each map the solid box indicates the LB FOV analysed in the text.

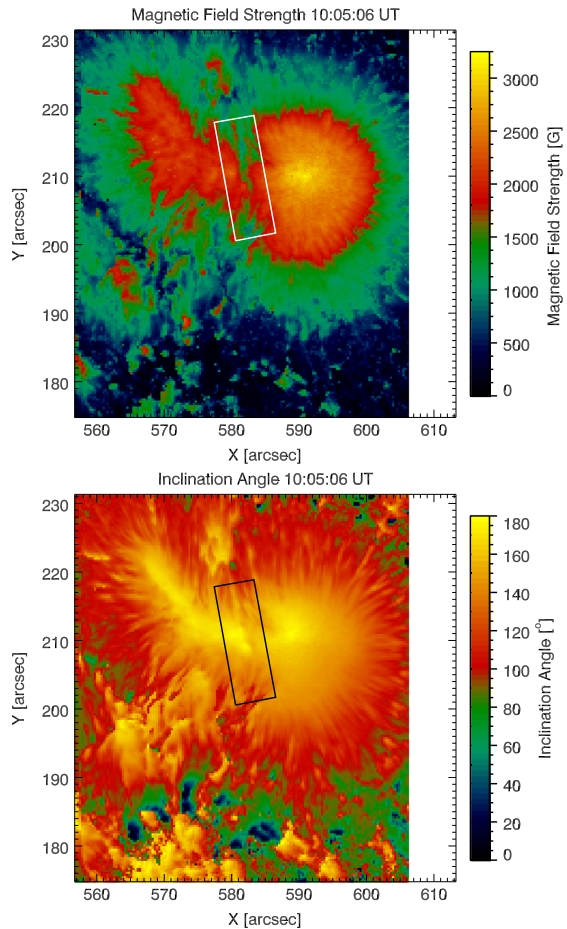


Figure 5 Continuum intensity map from CRISP observations of the LB with an overplotted black line indicating the position of the dark lane studied in the text (top panel) and the LOS plasma velocity values (bottom panels) estimated along the dark lane highlighted on the intensity map. North is on the left of the top image. The two white lines in the top panel and the two black lines in the bottom panel correspond to lines 1 and 2 reported in Figure 6. Positive (negative) values in velocity indicate motions away from (towards) the observer.

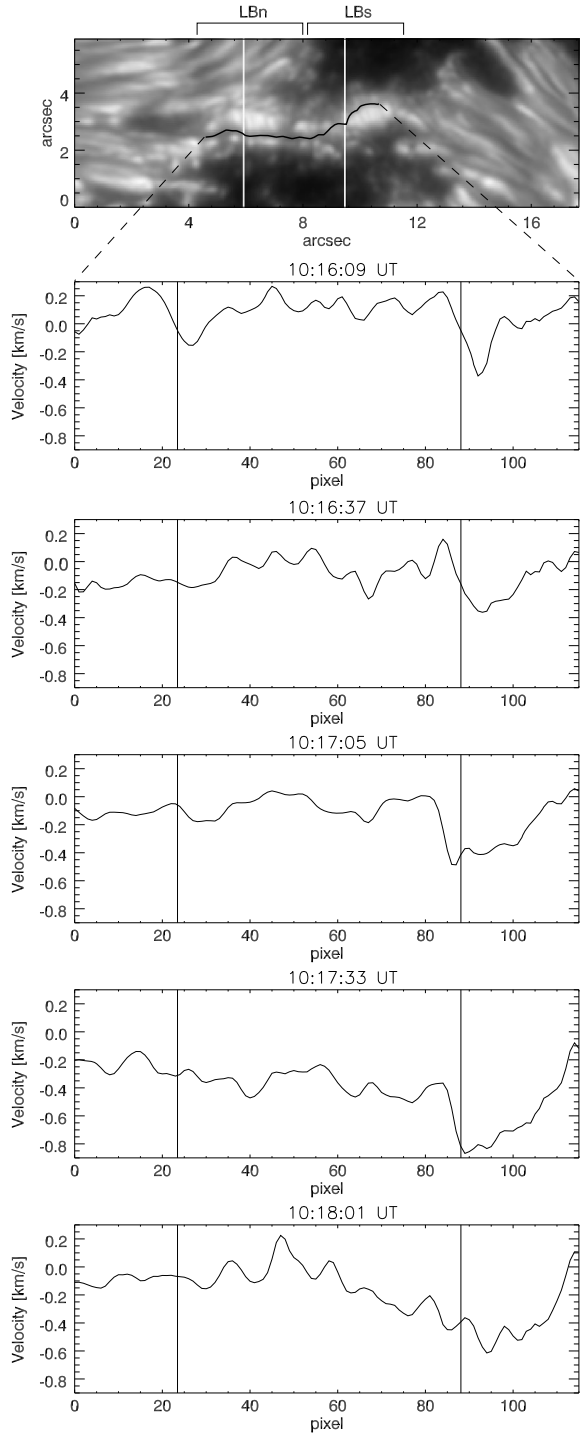
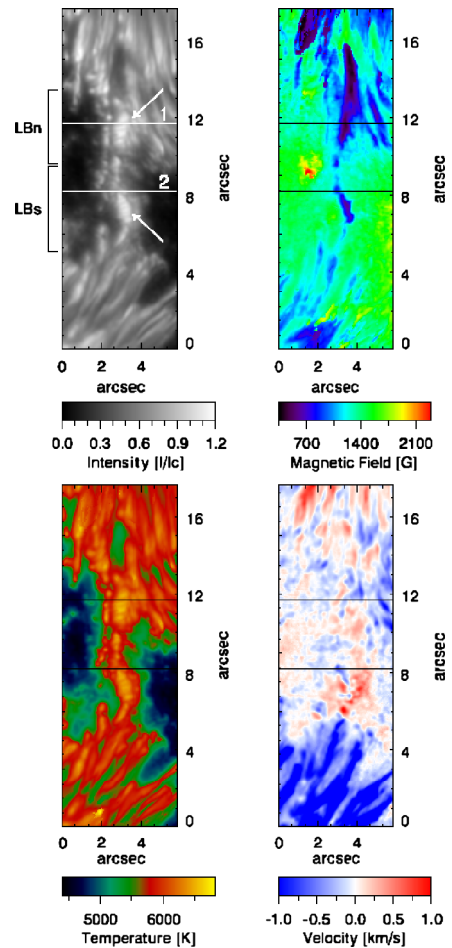


Figure 6 From top left, clockwise: maps of the normalised continuum intensity, magnetic field strength, LOS velocity and temperature of the region containing the LB, at 10:17 UT (CRISP dataset). The maps of the magnetic field strength and temperature have been obtained from the SIR inversion of the Stokes profiles along the Fe I 630.15 nm and 630.25 nm lines. In the LOS velocity map, derived from Gaussian fits, positive (negative) values correspond to motion away from the observer (towards the observer). The white lines in the intensity map and the dark lines in the other maps correspond to the pixels studied in Figure 7. In each map, line 1 indicates a region of LB_n and line 2 indicates a region of LB_s .



part of the LB). The maps of the magnetic field strength and of the temperature at $\log(\tau_5) = 0.0$ (where τ_5 is the optical depth at 500 nm) obtained by the SIR inversion (Figure 6, top right and bottom left panels) indicate that the granules of the LB that are characterised by a larger size correspond to regions with a weaker magnetic field and a higher temperature. The LOS velocity of the plasma along the LB is on average lower in value (of the order of $\approx \pm 0.6 \text{ km s}^{-1}$) than the LOS velocity in the neighbouring penumbral filaments, where the LOS component is of the order of $\approx 2 \text{ km s}^{-1}$ as a result of the Evershed flow (note that in Figure 6, bottom right panel, the LOS velocities are saturated between -1 and $+1 \text{ km s}^{-1}$ to highlight the LOS velocity values along the LB).

In Figure 7 we analyse the intensity, the magnetic field strength, the temperature, and the LOS velocity along the two segments perpendicular to the LB drawn in Figures 5 (bottom panel) and 6. The plots in the left and right columns of Figure 7 correspond to the above physical quantities along the segments in the northern and southern part of the LB, indicated in Figure 6 by labels 1 and 2, respectively. The vertical line in the plots indicates the location of the dark lane.

We note that the intensity of the dark lane is about $0.8 I/I_c$ for both parts of the LB (see Figure 7, top panels). In the LB_n (Figure 7, top left panel) we see that on both sides of the

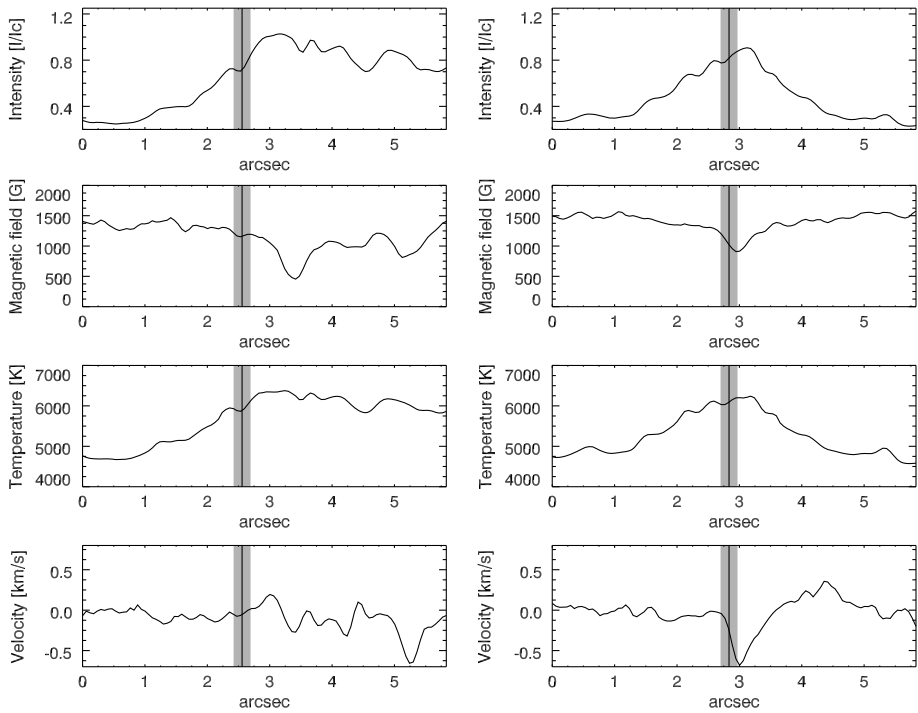


Figure 7 Left column: from top to bottom, plots of intensity, magnetic field strength, temperature, and LOS velocity along line 1 (see Figure 6). Right column: the same parameters along line 2 (see Figure 6). In these plots the black vertical line shows the dark lane position and the grey line shows its width.

dark lane there are two maxima in the continuum intensity. They correspond to the granules of the LB_n along line 1. The largest granule has a size of about $0.8''$ and is characterised by a magnetic field strength between 700 G and 1000 G (see Figure 7, second left panel). The smallest granule has a size of about $0.2''$ and a magnetic field of about 1500 G. The same behaviour is detected in the region selected in LB_s (see Figure 7, first two right panels). The temperature at $\log(\tau_5) = 0$ in the dark lane is about 6000 K (see Figure 7, third panel from the top), while the larger granules of the LB_n reach a temperature of about 6400 K.

In Figure 7 we note that the dark lane in the LB_n is almost at rest (see bottom left panel), while the granules at its sides are characterised by motion away from the observer (higher in the larger granule). The dark lane in the LB_s (see bottom right panel) shows motion toward the observer of the order of $\approx -0.6 \text{ km s}^{-1}$ and motion away from the observer between 0.1 and 0.4 km s^{-1} in the surrounding region. Moreover, in Figure 7 (bottom right panel) the motions toward the observer exceeding -0.5 km s^{-1} present a slight shift with respect to the location of the dark lane. This slight shift may be due to a foreshortening effect, taking into account that the AR is far from the central meridian.

To study the change in inclination angle inside and in the surroundings of the LB, we used the data acquired by *Hinode*/SP at 10:05 UT. In Figure 8 the *Hinode* maps of the continuum intensity and inclination angle, obtained using the MERLIN code, are shown for the region containing the LB. We studied the profile of the magnetic field inclination along the two segments drawn in Figure 6 and reported in blue and red in Figure 8. The inclination angle along the blue line of Figure 9 (which refers to the LB_n region, located between an

Figure 8 Maps of the intensity (left panel) and inclination angle (right panel) of the region containing the LB (see the solid box in Figure 3 indicating the analysed FOV for the LB deduced from *Hinode*/SP observations begun at 10:05 UT). The blue and red segments correspond to a part of the white lines 1 and 2, respectively, shown in Figure 6 (top left panel).

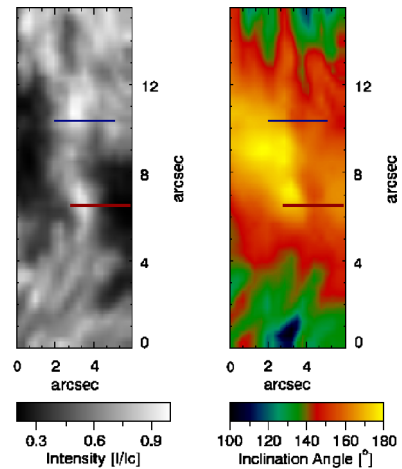
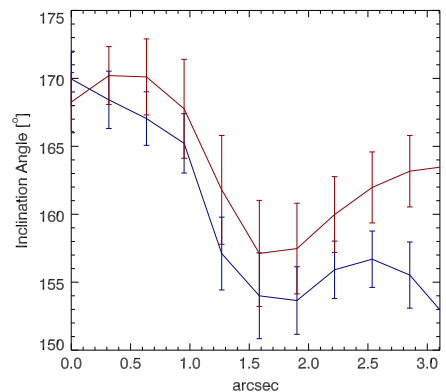


Figure 9 Plot of the inclination angle along the blue and red lines of Figure 8 and the respective error bars, corresponding to the 1σ uncertainty. The blue plot corresponds to the inclination angle along the LB_n located between an umbral and a penumbral zone. The red plot corresponds to the inclination angle along the LB_s located between two umbral cores.

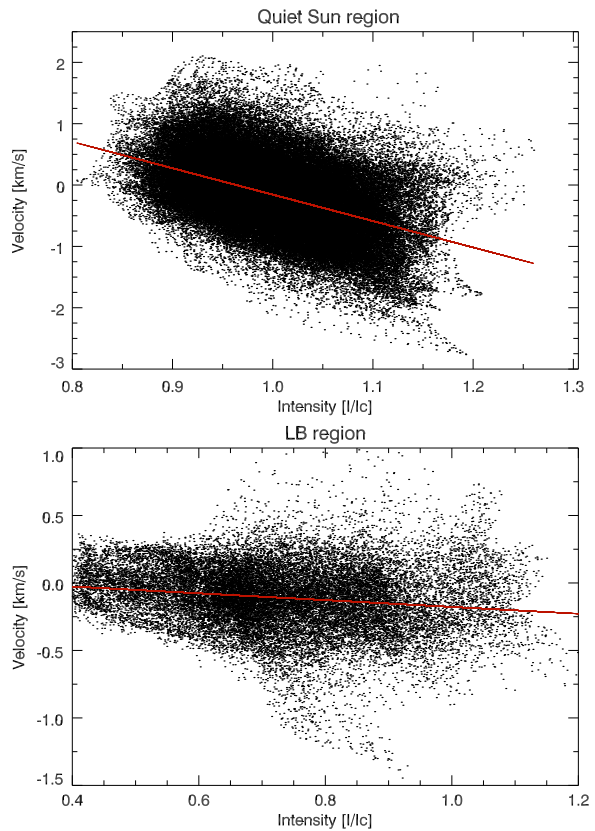


umbral region and a penumbral region) shows that in the eastern umbral region the magnetic field inclination has values around 170° , it reaches values lower than 155° in the centre of the LB_n and slightly more vertical values in the western penumbral region. In the LB_s (red line in Figure 9), located between two umbral regions, the inclination angle decreases to a minimum in the LB_s ($\approx 155^\circ$), but on both sides in the umbra the inclination angle is $\geq 165^\circ$. Given that MERLIN inversions do not provide the errors of the parameters, we estimated the errors of these measurements from inverting the *Hinode*/SP data using another Milne–Eddington-based code (Very Fast Inversion of the Stokes Vector (VFISV); Borrero *et al.*, 2011). The typical range of the standard deviation (1σ) for the inclination maps is between 2° and 5° . Thanks to this accuracy, we can also appreciate the small difference in the inclination in the two different regions of the LB.

4. Discussion

To interpret the LOS velocities found in the LB that we showed and analysed in Figures 5 and 7, we determined whether these motions towards or away from the observer may be

Figure 10 Scatter plots of intensity and LOS velocity in a region of the quiet-Sun (top panel) and in the region of the LB (bottom panel). The data shown in the latter plot include values of the five sequences studied in Figure 5. The red line in each plot represents the linear fit of the dataset.



related to upflows or downflows. We recall that in any position different from the disk centre ($\cos \theta = 0$), the LOS velocity is given by

$$v_{\text{LOS}} = v_z \cos \theta \pm v_h \sin \theta, \quad (1)$$

where v_z is the upflow or downflow (vertical) component, v_h is the horizontal component of the velocity, and θ is the heliocentric angle. To understand which velocity component prevails in the region of the LB, we produced a scatter plot of I/I_c and LOS velocity in a region of quiet-Sun (contained in the FOV) and in the LB region. Figure 10 (top panel) shows that there is a rather clear correlation ($r = -0.467$) in the quiet-Sun: brighter points, which correspond to areas occupied by granules that harbour upflows, show motions towards the observer, while darker points, corresponding to dark lanes that harbour downflows, show motions away from the observer. In a statistical sense, therefore, v_h is null and we can safely assume that LOS velocity in the quiet-Sun indicates upward or downward motions. Then, we checked if a comparable correlation might also be found in the region of the LB. However, in the scatter plot relevant to the LB region shown in Figure 10 (bottom panel), where we included the data of the five sequences studied in Figure 5 to increase statistics, we note only a very slight negative correlation ($r = -0.106$).

The latter result would seem to make us less confident that we can associate LOS velocities with upflows or downflows in the LB region. Nonetheless, we can further observe that even if we had $v_h \neq 0$, such a residual component can be neglected in our analysis.

It is known that LBs and penumbral filaments share a common origin (Spruit and Scharmer, 2006), therefore it might be expected that if there are high horizontal velocities in the LB, then they should be Evershed-like velocities. However, we do not observe such Evershed-like motions in the LOS map (see Figure 6, bottom right panel) towards the disk or the limb. Therefore, we are sure that Evershed-like horizontal motions do not affect our results. Furthermore, we note from Figure 3 that the direction of the main axis of the LB is almost perpendicular to the direction of the disk centre. Horizontal velocities perpendicular to the disk centre do not contribute to the measured LOS velocities because the angle between the LOS direction and v_h is 90° in such a configuration. Any residual v_h should be oriented along a direction parallel to the main axis of the LB, giving no contribution to the measured LOS velocity.

We can conclude that the LOS velocities that we studied have a vertical velocity component which prevails over the horizontal component and, then, we can also refer to these velocities as upflow and downflow plasma motions in the region of the LB.

5. Summary and Conclusions

Understanding the interplay between plasma convection and the magnetic field distribution in sunspot fine structure is fundamental to gain useful hints on the magneto-hydrodynamical processes occurring in the solar atmosphere and in the underlying layers, which are hidden from direct observations.

In this framework, this study is aimed at contributing to the understanding of the magnetic and kinematic properties of small-scale features observed in LBs. To accomplish this goal, we analysed CRISP data for a sequence acquired on 6 August 2011 at 10:17 UT along the Fe I line profile (630.15 nm and 630.25 nm). The FOV of interest contains the preceding, negative polarity sunspot of AR NOAA 11263, where, according to HMI/SDO data analysis, an LB had formed in the previous days. The sunspot was in the decaying phase, and an LB is evidence of the re-establishment of the granulation within the spot. The LB is quite defined and presents a granular morphology, with a dark lane along all the length of its main axis; according to Sobotka, Bonet, and Vazquez (1994), this LB is a strong light bridge (SLB).

From investigating the continuum intensity images of the sequence acquired by CRISP at 10:17 UT, during the best seeing conditions, we confirm that the LB was segmented: it was characterised by a central dark lane having at its sides granules of different sizes separated by tiny intergranular lanes. The LB was an interesting target because it was characterised by a different configuration at its sides along its length: the southern part was located between two umbral cores, while the northern part was located between an umbral core on one side and penumbral filaments on the other side.

Using the CRISP data, we analysed the thermal and kinematic properties separately for the upper and lower parts of the LB located between the umbral and the penumbral filaments (LB_n) and between the dark umbral cores (LB_s), respectively. In the LB_n there are grains of different size along the dark lane: grains in the western part have a size of about $0.8''$ and a magnetic field of ≈ 700 G, while the grains in the eastern part have a size of about $0.2''$ and a magnetic field of ≈ 1500 G. In the LB_s the grains on the eastern side of the dark lane are larger. The width of the dark lane is about $0.3''$, in agreement with the results obtained by Berger and Berdyugina (2003). Furthermore, we found that the intensity of the LB granules is about $0.9 I/I_c$.

The results of this analysis, shown in Figure 7, indicate that in both portions of the LB the dark lane has an intensity of $0.8 I/I_c$ and a temperature at $\log(\tau_5) = 0$ of about 6000 K.

Nordlund and Scharmer (2010) found a cusp-shaped central dark lane in an LB formed in a three-dimensional MHD simulation of a field-free gap surrounded by an umbral-like atmosphere and predicted that the dark lane in sunspot LBs harbours upflows. It is challenging to observationally confirm these outcomes, which were derived from numerical simulations. High spatial resolution observations have shown that LBs are highly spatially structured, with convective motions occurring on spatial scales of a few arcseconds. The mixing of information from these features, if not resolved, can thus lead to incorrect estimates of the sign of the plasma velocities, thus explaining the discrepancy of results reported in the literature (Rimmele, 1997).

Moreover, we observed a different behaviour in the plasma motions in the LB_s and LB_n , characterised by different magnetic field configurations in the surroundings. The LB_s is located between two regions with almost vertical magnetic fields (see the red plot in Figure 9). The dark lane in this region hosts motions towards the observer with LOS velocities between -0.2 and -0.6 km s^{-1} , as shown also in Figure 5. This last finding is in agreement with the results of Ruppe van der Voort, Bellot Rubio, and Ortiz (2010) and confirms the hypothesis that the dark lane is a cusp-like region where the plasma piles up as a consequence of the braking of vertical flows. On the other hand, LB_n is located between regions with an almost vertical magnetic field on one side and a more inclined field on the other side (see the blue plot in Figure 9). The dark lane in this region shows weaker motions towards the observer, probably indicating that the process of plasma pile-up in this condition is somehow modified.

Therefore, we conclude that the configuration of the surrounding magnetic field can play an important role not only in the formation of a cusp-like region with enhanced density and corresponding to the dark lane, but also in the vertical upflow that is usually observed along these structures. The results obtained from our study thus support recent MHD simulations and observations of magneto-convection in sunspot atmospheres.

Acknowledgements We are grateful to the University of Catania for providing the funds necessary to carry out the Observational Campaign in La Palma. The 1-m *Swedish Solar Telescope* is operated on the island of La Palma by the Institute for Solar Physics (ISP) of Stockholm University in the Spanish Observatorio del Roque de los Muchachos of the Instituto de Astrofísica de Canarias. *Hinode* is a Japanese mission developed and launched by ISAS/JAXA, with NAOJ as domestic partner and NASA and STFC (UK) as international partners. It is operated by these agencies in co-operation with ESA and NSC (Norway). The HMI/SDO data used in this paper are courtesy of NASA/SDO and the HMI science team. Use of NASA's Astrophysical Data System is gratefully acknowledged. We are grateful to Dr. Rolf Schlichenmaier for the useful discussions and helpful suggestions. This research has received funding from the EC 7th Framework Programme FP7/2007-2013 under the grant agreement eHEROES (project n. 284461). We are grateful to the SOLARNET project for providing the grant for the Young Researches Mobility (project n. 312495). This work was also supported by the Instituto Nazionale di Astrofisica (PRIN INAF 2014), and by the University of Catania (PRIN MIUR 2012).

References

- Asai, A., Ishii, T.T., Kurokawa, H.: 2001, Plasma ejections from a light bridge in a sunspot umbra. *Astrophys. J.* **555**, L65. DOI. ADS.
- Balthasar, H., Schmidt, W.: 1993, Polarimetry and spectroscopy of a simple sunspot. 2: On the height and temperature dependence of the magnetic field. *Astron. Astrophys.* **279**, 243. ADS.
- Berger, T.E., Berdyugina, S.V.: 2003, The observation of sunspot light-bridge structure and dynamics. *Astrophys. J.* **589**, L117. DOI. ADS.
- Borrero, J.M., Ichimoto, K.: 2011, Magnetic structure of sunspots. *Living Rev. Solar Phys.* **8**, 4. DOI. ADS.
- Borrero, J.M., Tomczyk, S., Kubo, M., Socas-Navarro, H., Schou, J., Couvidat, S., Bogart, R.: 2011, VFISV: Very Fast Inversion of the Stokes Vector for the helioseismic and magnetic imager. *Solar Phys.* **273**, 267. DOI. ADS.

- Collados, M., Martínez Pillet, V., Ruiz Cobo, B., del Toro Iniesta, J.C., Vázquez, M.: 1994, Observed differences between large and small sunspots. *Astron. Astrophys.* **291**, 622. [ADS](#).
- Cowling, T.G.: 1957, *Magnetohydrodynamics*, Interscience Publishers, Inc., New York.
- Cristaldì, A., Guglielmino, S.L., Zuccarello, F., Romano, P., Falco, M., Rouppe van der Voort, L., de la Cruz Rodríguez, J., Ermolli, I., Criscuoli, S.: 2014, Dynamic properties along the neutral line of a delta spot inferred from high-resolution observations. *Astrophys. J.* **789**, 162. [DOI](#). [ADS](#).
- de la Cruz Rodríguez, J., Löfdahl, M.G., Sütterlin, P., Hillberg, T., Rouppe van der Voort, L.: 2015, CRISPRED: A data pipeline for the CRISP imaging spectropolarimeter. *Astron. Astrophys.* **573**, A40. [DOI](#). [ADS](#).
- del Toro Iniesta, J.C., Tarbell, T.D., Ruiz Cobo, B.: 1994, On the temperature and velocity through the photosphere of a sunspot penumbra. *Astrophys. J.* **436**, 400. [DOI](#). [ADS](#).
- Georgoulis, M.K.: 2005, A new technique for a routine azimuth disambiguation of solar vector magnetograms. *Astrophys. J.* **629**, L69. [DOI](#). [ADS](#).
- Giordano, S., Berrilli, F., Del Moro, D., Penza, V.: 2008, The photospheric structure of a solar pore with light bridge. *Astron. Astrophys.* **489**, 747. [DOI](#). [ADS](#).
- Hirzberger, J., Bonet, J.A., Sobotka, M., Vázquez, M., Hanslmeier, A.: 2002, Fine structure and dynamics in a light bridge inside a solar pore. *Astron. Astrophys.* **383**, 275. [DOI](#). [ADS](#).
- Jurčák, J., Martínez Pillet, V., Sobotka, M.: 2006, The magnetic canopy above light bridges. *Astron. Astrophys.* **453**, 1079. [DOI](#). [ADS](#).
- Jurčák, J., Sobotka, M., Martínez Pillet, V.: 2005, The magnetic configuration in light bridges. In: *The Dynamic Sun: Challenges for Theory and Observations, ESA Special Publication* **600**, 8.1. [ADS](#).
- Katsukawa, Y., Yokoyama, T., Berger, T.E., Ichimoto, K., Kubo, M., Lites, B., Nagata, S., Shimizu, T., Shine, R.A., Suematsu, Y., Tarbell, T.D., Title, A.M., Tsuneta, S.: 2007, Formation process of a light bridge revealed with the Hinode solar optical telescope. *Publ. Astron. Soc. Japan* **59**, S577. [DOI](#). [ADS](#).
- Kosugi, T., Matsuzaki, K., Sakao, T., Shimizu, T., Sone, Y., Tachikawa, S., Hashimoto, T., Minesugi, K., Ohnishi, A., Yamada, T., Tsuneta, S., Hara, H., Ichimoto, K., Suematsu, Y., Shimojo, M., Watanabe, T., Shimada, S., Davis, J.M., Hill, L.D., Owens, J.K., Title, A.M., Culhane, J.L., Harra, L.K., Doschek, G.A., Golub, L.: 2007, The Hinode (Solar-B) mission: An overview. *Solar Phys.* **243**, 3. [DOI](#). [ADS](#).
- Leka, K.D.: 1997, The vector magnetic fields and thermodynamics of sunspot light bridges: The case for field-free disruptions in sunspots. *Astrophys. J.* **484**, 900. [ADS](#).
- Lites, B.W., Bida, T.A., Johannesson, A., Scharmer, G.B.: 1991, High-resolution spectra of solar magnetic features. II – Magnetic fields of umbral brightenings. *Astrophys. J.* **373**, 683. [DOI](#). [ADS](#).
- Lites, B.W., Scharmer, G.B., Berger, T.E., Title, A.M.: 2004, Three-dimensional structure of the active region photosphere as revealed by high angular resolution. *Solar Phys.* **221**, 65. [DOI](#). [ADS](#).
- Lites, B.W., Akin, D.L., Card, G., Cruz, T., Duncan, D.W., Edwards, C.G., Elmore, D.F., Hoffmann, C., Katsukawa, Y., Katz, N., Kubo, M., Ichimoto, K., Shimizu, T., Shine, R.A., Stander, K.V., Suematsu, A., Tarbell, T.D., Title, A.M., Tsuneta, S.: 2013, The Hinode spectro-polarimeter. *Solar Phys.* **283**, 579. [DOI](#). [ADS](#).
- Lites, B., Casini, R., Garcia, J., Socas-Navarro, H.: 2007, A suite of community tools for spectro-polarimetric analysis. *Mem. Soc. Astron. Ital.* **78**, 148. [ADS](#).
- Louis, R.E., Beck, C., Ichimoto, K.: 2014, Small-scale chromospheric jets above a sunspot light bridge. *Astron. Astrophys.* **567**, A96. [DOI](#). [ADS](#).
- Markwardt, C.B.: 2009, Non-linear least-squares fitting in IDL with MPFIT. In: Bohlender, D.A., Durand, D., Dowler, P. (eds.) *Astronomical Data Analysis Software and Systems XVIII, Astronomical Society of the Pacific Conference Series* **411**, 251. [ADS](#).
- Nordlund, Å., Scharmer, G.B.: 2010, Convection and the origin of Evershed flows. *Astrophys. Space Sci. Proc.* **19**, 243. [DOI](#). [ADS](#).
- Parker, E.N.: 1979a, Sunspots and the physics of magnetic flux tubes. I – The general nature of the sunspot. II – Aerodynamic drag. *Astrophys. J.* **230**, 905. [DOI](#). [ADS](#).
- Parker, E.N.: 1979b, Sunspots and the physics of magnetic flux tubes. II. Aerodynamic drag. *Astrophys. J.* **230**, 914. [ADS](#).
- Parker, E.N.: 1979c, Sunspots and the physics of magnetic flux tubes. III – Aerodynamic lift. *Astrophys. J.* **231**, 250. [DOI](#). [ADS](#).
- Pesnell, W.D., Thompson, B.J., Chamberlin, P.C.: 2012, The Solar Dynamics Observatory (SDO). *Solar Phys.* **275**, 3. [DOI](#). [ADS](#).
- Rempel, M., Schlichenmaier, R.: 2011, Sunspot modeling: From simplified models to radiative MHD simulations. *Living Rev. Solar Phys.* **8**, 3. [DOI](#). [ADS](#).
- Rimmele, T.: 2008, On the relation between umbral dots, dark-cored filaments, and light bridges. *Astrophys. J.* **672**, 684. [DOI](#). [ADS](#).
- Rimmele, T.R.: 1997, Evidence for magnetoconvection in a sunspot light bridge. *Astrophys. J.* **490**, 458. [ADS](#).

- Roupe van der Voort, L., Bellot Rubio, L.R., Ortiz, A.: 2010, Upflows in the central dark lane of sunspot light bridges. *Astrophys. J.* **718**, L78. DOI. ADS.
- Ruiz Cobo, B., del Toro Iniesta, J.C.: 1992, Inversion of Stokes profiles. *Astrophys. J.* **398**, 375. DOI. ADS.
- Scharmer, G.B., Bjelksjo, K., Korhonen, T.K., Lindberg, B., Petterson, B.: 2003, The 1-meter Swedish solar telescope. In: Keil, S.L., Avakyan, S.V. (eds.) *Innovative Telescopes and Instrumentation for Solar Astrophysics, Proc. SPIE* **4853**, 341. ADS.
- Scharmer, G.B., Narayan, G., Hillberg, T., de la Cruz Rodriguez, J., Löfdahl, M.G., Kiselman, D., Sütterlin, P., van Noort, M., Lagg, A.: 2008, CRISP spectropolarimetric imaging of penumbral fine structure. *Astrophys. J.* **689**, L69. DOI. ADS.
- Scherrer, P.H., Schou, J., Bush, R.I., Kosovichev, A.G., Bogart, R.S., Hoeksema, J.T., Liu, Y., Duvall, T.L., Zhao, J., Title, A.M., Schrijver, C.J., Tarbell, T.D., Tomczyk, S.: 2012, The Helioseismic and Magnetic Imager (HMI) Investigation for the Solar Dynamics Observatory (SDO). *Solar Phys.* **275**, 207. DOI. ADS.
- Schnerr, R.S., de La Cruz Rodríguez, J., van Noort, M.: 2011, Stokes imaging polarimetry using image restoration: A calibration strategy for Fabry–Pérot based instruments. *Astron. Astrophys.* **534**, A45. DOI. ADS.
- Schüssler, M., Vögler, A.: 2006, Magnetoconvection in a sunspot umbra. *Astrophys. J.* **641**, L73. DOI. ADS.
- Shimizu, T.: 2011, Long-term evolution of magnetic and dynamical properties in a sunspot light bridge. *Astrophys. J.* **738**, 83. DOI. ADS.
- Shimizu, T., Katsukawa, Y., Kubo, M., Lites, B.W., Ichimoto, K., Suematsu, Y., Tsuneta, S., Nagata, S., Shine, R.A., Tarbell, T.D.: 2009, Hinode observation of the magnetic fields in a sunspot light bridge accompanied by long-lasting chromospheric plasma ejections. *Astrophys. J.* **696**, L66. DOI. ADS.
- Sobotka, M., Bonet, J.A., Vazquez, M.: 1994, A high-resolution study of the structure of sunspot light bridges and abnormal granulation. *Astrophys. J.* **426**, 404. DOI. ADS.
- Spruit, H.C., Scharmer, G.B.: 2006, Fine structure, magnetic field and heating of sunspot penumbrae. *Astron. Astrophys.* **447**, 343. DOI. ADS.
- Thomas, J.H., Weiss, N.O.: 2004, Fine structure in sunspots. *Annu. Rev. Astron. Astrophys.* **42**, 517. DOI. ADS.
- Toriumi, S., Katsukawa, Y., Cheung, M.C.M.: 2015, Light bridge in a developing active region. I. Observation of light bridge and its dynamic activity phenomena. *Astrophys. J.* **811**, 137. DOI. ADS.
- Tsuneta, S., Ichimoto, K., Katsukawa, Y., Nagata, S., Otsubo, M., Shimizu, T., Suematsu, Y., Nakagiri, M., Noguchi, M., Tarbell, T., Title, A., Shine, R., Rosenberg, W., Hoffmann, C., Jurcevich, B., Kushner, G., Levay, M., Lites, B., Elmore, D., Matsushita, T., Kawaguchi, N., Saito, H., Mikami, I., Hill, L.D., Owens, J.K.: 2008, The solar optical telescope for the Hinode mission: An overview. *Solar Phys.* **249**, 167. DOI. ADS.
- van Noort, M., Roupe van der Voort, L., Löfdahl, M.G.: 2005, Solar image restoration by use of multi-frame blind de-convolution with multiple objects and phase diversity. *Solar Phys.* **228**, 191. DOI. ADS.
- Vazquez, M.: 1973, A morphological study of the light-bridges in sunspots. *Solar Phys.* **31**, 377. DOI. ADS.